

A reliable Padé analytical continuation method based on a high accuracy symbolic computation algorithm

K. S. D. Beach[†], R. J. Gooding

Dept. of Physics, Queen's University, Kingston, Ontario, Canada K7L 3N6

F. Marsiglio

Dept. of Physics, University of Alberta, Edmonton, Alberta, Canada T6G 2J1

(February 14, 2019)

We critique a Padé analytic continuation method whereby a rational polynomial function is fit to a set of input points by means of a single matrix inversion. This procedure is accomplished to an extremely high accuracy using a novel symbolic computation algorithm. As an example of this method in action it is applied to the problem of determining the spectral function of a single-particle thermal Green's function known only at a finite number of Matsubara frequencies with two example self energies drawn from the T-matrix theory of the Hubbard model. We present a systematic analysis of the effects of error in the input points on the analytic continuation, and this leads us to propose a procedure to test quantitatively the reliability of the resulting continuation, thus eliminating the black magic label frequently attached to this procedure.

I. INTRODUCTION

Analytic continuation arises in the many-body problem whenever real time dynamics are to be recovered from a response function calculated at non-zero temperatures in the Matsubara formalism. In that case, the function whose value is known only at a discrete set of points on the imaginary axis must be continued to the real axis.

A general statement of the problem of interest in this paper is as follows: An analytic continuation of a function f defined on a subset $\mathcal{A} \subset \mathbb{C}$ is a function that coincides with f on \mathcal{A} and is analytic on a domain containing \mathcal{A} . Usually, we are interested in the analytic continuation \bar{f} with the largest such domain, for then \bar{f} is the greatest analytic extension of f to the complex plane. Since there exists no general prescription for finding \bar{f} from f , there is no choice but to resort to approximate techniques. Currently, the state of the “art” is to interpolate between known points using fitting functions capable of reproducing the analytic structure of \bar{f} in the complex plane¹. A serious difficulty is that the analytic structure of \bar{f} is not usually known a priori.

A widely used technique is the Padé approximant method in which ratios of polynomials (or terminating continued fractions) are used as fitting functions. Several Padé schemes exist. The most common scheme, a

recursive algorithm called Thiele's Reciprocal Difference Method², was used by Vidberg and Serene³ in the context of the Eliashberg equations. Yet, despite twenty years of widespread use, the Padé approximant method remains somewhat of an untested approach in that there is still no reliable, quantitative measure of the quality of a Padé result. The prevailing wisdom is that a Padé fit can be considered ‘good’ when the output function is stable with respect to the addition of more input points. The results of this work make it clear that such a criterion is insufficient.

The various Padé schemes can be divided into two broad classes: (I) those which return the value of the continued function point by point in the complex plane ($f(\mathcal{A}, z) \mapsto \bar{f}(z)$) and (II) those which yield the function itself $f(\mathcal{A}) \mapsto \bar{f}$ by returning the polynomial (or continued fraction) coefficients. Thiele's method is class I, as are most numerical methods. In this work we present a robust Padé scheme that is class II and propose a goodness-of-fit criterion based on the convergence of the polynomial coefficients to allowed values. One advantage of our approach is that we formulate the problem as a matrix equation, allowing us to make use of existing, highly efficient routines for matrix inversion. In contrast, a naïvely implemented recursion algorithm can lead to a severe propagation of error since repeated operations are performed on terms of very different orders of magnitude.

Our paper is organized as follows. In the next section we review the formal aspects of thermal Green's functions to establish the definitions of the various functions that enter into this problem. In §III we present the details of the Padé form that we will use, and state the algorithm that we use to solve for the Padé coefficients. This leads to the consideration of the accuracy required for such a calculation, thus necessitating the use of a high accuracy symbolic computation algorithm. This is presented in §IV, and then we display our numerical results for relevant test functions, including the statistical test that allows us to conclude whether or not a given analytic continuation is accurate. Finally, in §V we present our conclusions.

II. GREEN'S FUNCTION FORMALISM

First, we introduce the components of theories based on thermal Green's functions to establish the definitions of the various functions that enter into this problem.

The one-particle propagator or Green's function can be formulated using real or imaginary time operators. In real time, the retarded Green's function

$$G^{\text{R}}(t) = -i\langle\{c(it), c^\dagger(0)\}\theta(t)\rangle \quad (1)$$

describes how the system responds when a particle is added at time zero and removed at time t . Its imaginary time counterpart, the thermal Green's function

$$G(\tau) = -\langle\mathbb{T}[c(\tau)c^\dagger(0)]\rangle, \quad (2)$$

is not so clearly physically motivated. Its main advantages are its mathematical elegance and computational ease. Further, since it is defined in terms of the time ordering operator \mathbb{T} , $G(\tau)$ admits a diagrammatic expansion via Wick's theorem. Moreover, whereas the retarded Green's function $G^{\text{R}}(t)$ is aperiodic in t (it has a lone discontinuity at $t = 0$), the temperature Green's function is periodic in τ with period 2β .

The two Green's functions have Fourier representations: the first a Fourier transform

$$G^{\text{R}}(t) = \frac{1}{2\pi} \int_{-\infty}^{\infty} d\omega e^{-i\omega t} G^{\text{R}}(\omega) \quad (3)$$

and the second, as a consequence of its periodicity, a Fourier series

$$G(\tau) = \frac{1}{\beta} \sum_{\text{odd } m} e^{-im\pi\tau/\beta} G_m \quad (4)$$

$$= \frac{1}{\beta} \sum_{\omega_n} e^{-i\omega_n\tau} G(\omega_n) \quad (5)$$

which, in Eq. (5), we have recast as a sum over the Matsubara frequencies $\{\omega_n = (2n - 1)\pi/\beta : n \in \mathbb{Z}\}$ of some new Fourier component $G(\omega_n)$.

The formal connection between the real and imaginary time formalisms is the following: There exists a unique function $\bar{G} : \mathbb{C} \mapsto \mathbb{C}$ with asymptotic form

$$\bar{G}(z) = (1/z)(1 + \mathcal{O}(1/\text{Im } z)) \quad (6)$$

which takes on the values of the Fourier components of the temperature Green's function at Matsubara points on the imaginary axis $\bar{G}(i\omega_n) = G(\omega_n)$ and gives the Fourier transform of the retarded Green's function just above the real axis $\bar{G}(\omega + i0^+) = G^{\text{R}}(\omega)$. That is, Eqs. (3) and (5) can be written as

$$G^{\text{R}}(t) = \frac{1}{2\pi} \int_{-\infty}^{\infty} d\omega e^{-i\omega t} \bar{G}(\omega + i0^+) \quad (7)$$

and

$$G(\tau) = \frac{1}{\beta} \sum_{\omega_n} e^{-i\omega_n\tau} \bar{G}(i\omega_n). \quad (8)$$

Clearly, all the information one can potentially extract from these functions is contained in \bar{G} .

The function \bar{G} has several interesting properties. First, it is analytic everywhere in the complex plane with the exception of the real axis; this is a causality requirement. Second, the value of \bar{G} in the upper and lower half planes is related by $\bar{G}(z^*) = \bar{G}(z)^*$, which is a statement of the time reversal symmetry between the retarded and advanced Green's functions. Its immediate consequence is that the imaginary part of \bar{G} may be discontinuous across the real axis. It also implies that we need only know the function in either the upper or the lower half plane since the other is a conjugated reflection of the first. Third, \bar{G} can be written as a Stieltjes/Hilbert transform

$$\bar{G}(z) = \int_{-\infty}^{\infty} d\omega \frac{A(\omega)}{z - \omega} \quad (9)$$

where the spectral function, given by the magnitude of the discontinuity in \bar{G} across the real axis, viz.

$$\begin{aligned} A(\omega) &= -\frac{1}{\pi} \text{Im } G^{\text{R}}(\omega) \\ &= -\frac{1}{2\pi i} (\bar{G}(\omega + i0^+) - \bar{G}(\omega - i0^+)), \end{aligned} \quad (10)$$

is non-negative and normalized to unity

$$A(\omega) \geq 0, \quad \int_{-\infty}^{\infty} d\omega A(\omega) = 1. \quad (11)$$

Typically, we are working in the Matsubara formalism and we calculate $G(\omega_n)$ from its self-energy (via $G(\omega_n)^{-1} = i\omega_n - \xi - \Sigma(\omega_n)$) which is in turn calculated from an approximate theory based on, e.g., a diagrammatic expansion of the propagator. From here the route to real time dynamics is somewhat circuitous:

$$G(\omega_n) \xrightarrow{1} \bar{G}(z) \xrightarrow{2} G^{\text{R}}(\omega) \xrightarrow{3} G^{\text{R}}(t). \quad (12)$$

(1) The first step is to analytically continue from the Fourier components of the temperature Green's function to construct \bar{G} . That this is possible, in principle, provided we know $G(\omega_n) = \bar{G}(i\omega_n)$ for an infinite set of points including the point at infinity, was proved by Baym and Mermin⁴. (2) Supposing that the analytic continuation to the upper half plane can be found, we merely evaluate it along the real axis (setting $z = \omega + i0^+$) to get $G^{\text{R}}(\omega)$. (3) A Fourier transform then recovers the real time response function.

In practice, however, we do not know the values of $G(\omega_n)$ at an infinite number of points. Moreover, even if we did, the theorem of Baym and Mermin shows only the existence of a function \bar{G} . There is no general method to perform the analytic continuation — hence the need for a procedure such as the Padé.

III. PADÉ APPROXIMANTS

The Padé method is based on the assumption that \bar{G} can be written as a rational polynomial or terminating continued fraction. Since theories are most commonly specified by a choice of self-energy, the continued fraction form turns out to be the more useful, at least for investigating questions of a mathematical nature (e.g. analytic structure). In particular, we shall find it helpful to consider \bar{G} (in the upper half plane) a continued fraction of Jacobi form^{5,6} (J-frac). That is,

$$\bar{G}(z) = \bar{G}_{(r+1)}(z) = \frac{\lambda_0^2}{z - e_0} \frac{\lambda_1^2}{z - e_1} \cdots \frac{\lambda_r^2}{z - e_r} \quad (13)$$

$$= \frac{1}{z - \xi - \bar{\Sigma}_{(r)}(z)} \quad (14)$$

where the λ_n and e_n are complex constants. By comparison with Dyson's equation, Eq. (14), we make the identification $\lambda_0^2 = 1$ and $e_0 = \xi$, where ξ is just the free particle energy measured with respect to the chemical potential⁷. Then, we find that $\bar{\Sigma}_{(r)}(z)$ is itself a continued fraction

$$\bar{\Sigma}_{(r)}(z) = \frac{\lambda_1^2}{z - e_1} \frac{\lambda_2^2}{z - e_2} \cdots \frac{\lambda_r^2}{z - e_r}. \quad (15)$$

The justification for this continued fraction form is a theorem due to Wall and Wetzel⁸ which assures us that a positive definite J-frac has a spectral representation with non-negative, integrable spectral weight and that it is analytic in the upper half complex plane — all the properties we know \bar{G} must have to be physically reasonable. By positive definite J-frac we mean a continued fraction in the form of Eq. (13) satisfying $\text{Im } e_n \leq 0$ and for which there exists a sequence of real numbers g_0, g_1, \dots ($0 \leq g_n \leq 1$) such that

$$(\text{Im } \lambda_n)^2 = (\text{Im } e_{n-1})(\text{Im } e_n)(1 - g_{n-1})g_n. \quad (16)$$

There are two special cases worth mentioning. If the λ_n and e_n are all real then the J-frac is positive definite and can be cast as a sum of simple poles⁵

$$\sum_{n=1}^r \frac{R_n}{z - E_n} \quad (17)$$

with real, distinct energies E_n and positive residues $R_n > 0$. The J-frac is also positive definite if the λ_n are real and none of the e_n sits in the upper half complex plane (Eq. (16) is satisfied by setting all $g_n = 0$ or 1), in which case the function is characterized by simple poles resting on or below the real axis. In the general case, all the continued fraction coefficients have the potential to be complex, with the exception of $\lambda_0^2 = 1$, $e_0 = \xi$, and λ_1^2 . Since $e_0 = \xi$ has no imaginary part, Eq. (16) implies that the coefficient λ_1^2 must always be real and positive.

It is clear that by observing the values of the λ_n, e_n coefficients, one can learn a great deal about the analytic

properties of $\bar{G}_{(r+1)}$. For example, if some e_n has a positive imaginary part (and no $\lambda_m = 0$ for $m < n$) then $\bar{G}_{(r+1)}$ may have a pole in the upper half plane — such a function would be noncausal and have negative spectral weight. (In fact, it is through such considerations that we are led to propose a method for testing the accuracy of a given analytic continuation via a Padé.)

Nonetheless, despite the usefulness of the continued fraction form, for computational purposes it is actually much easier to work with rational polynomials. Conveniently, every terminating continued fraction is equivalent to a rational polynomial. For instance, a J-frac with r stories, Eq. (15) say, can be written as the ratio

$$\bar{\Sigma}_{(r)}(z) = \frac{P_{(r)}(z)}{Q_{(r)}(z)} \quad (18)$$

of two polynomials P, Q defined recursively by the formulas

$$P_{(n+1)} = (z - e_n)P_{(n)}(z) - \lambda_n^2 P_{(n-1)}(z) \quad (19a)$$

$$Q_{(n+1)} = (z - e_n)Q_{(n)}(z) - \lambda_n^2 Q_{(n-1)}(z) \quad (19b)$$

(for $n = 1, 2, 3, \dots$) with base cases

$$P_{(0)} = 0, P_{(1)} = \lambda_1^2 \quad (20a)$$

$$Q_{(0)} = 1, Q_{(1)} = z - e_1. \quad (20b)$$

Writing out the leading order terms of P and Q

$$P_{(r)}(z) = \lambda_1^2 z^{r-1} - \lambda_1^2 (e_2 + e_3 + \cdots + e_r) z^{r-2} + \cdots \quad (21a)$$

$$Q_{(r)}(z) = z^r - (e_1 + e_2 + \cdots + e_r) z^{r-1} + \cdots \quad (21b)$$

makes it clear that the polynomial P is of order $r - 1$ in z while the polynomial Q is of order r . (Accordingly, one refers to $\bar{\Sigma}_{(r)}$ in Eq. (18) as a $[r - 1/r]$ rational polynomial.) Moreover, it suggests that we write the self energy explicitly as a rational polynomial of the form

$$\bar{\Sigma}_{(r)}(z) = \frac{p_1 + p_2 z + \cdots + p_r z^{r-1}}{q_1 + q_2 z + \cdots + q_r z^{r-1} + z^r}. \quad (22)$$

It is straightforward to relate the old and new coefficients to one another via Eqs. (19) and (20): e.g. $\lambda_1^2 = p_r$, $e_1 = p_{r-1}/p_r - q_r$, etc.

The coefficients p_n, q_n can be determined by specifying the value of $\bar{\Sigma}_{(r)}$ at $2r$ points, *viz.*, by solving the set of $2r$ linear equations⁹

$$\{\bar{\Sigma}_{(r)}(i\omega_n) = \Sigma(\omega_n)\}. \quad (23)$$

If we define the column vectors

$$\begin{bmatrix} \mathbf{p} \\ \mathbf{q} \end{bmatrix} = \begin{bmatrix} p_1 \\ \vdots \\ p_r \\ q_1 \\ \vdots \\ q_r \end{bmatrix} \quad \text{and} \quad \tilde{\sigma} = \begin{bmatrix} \sigma_1(i\omega_1)^r \\ \sigma_2(i\omega_2)^r \\ \vdots \\ \sigma_{2r}(i\omega_{2r})^r \end{bmatrix}, \quad (24)$$

where $\sigma_n = \Sigma(\omega_n)$ are the known values of the self-energy at $2r$ Matsubara frequencies, and a matrix

$$X = \begin{bmatrix} 1 & i\omega_1 & \cdots & (i\omega_1)^{r-1} & -\sigma_1 & \cdots & -\sigma_1(i\omega_1)^{r-1} \\ 1 & i\omega_2 & \cdots & (i\omega_2)^{r-1} & -\sigma_2 & \cdots & -\sigma_2(i\omega_2)^{r-1} \\ \vdots & \vdots & \ddots & \vdots & \vdots & \ddots & \vdots \\ 1 & i\omega_{2r} & \cdots & (i\omega_{2r})^{r-1} & -\sigma_{2r} & \cdots & -\sigma_{2r}(i\omega_{2r})^{r-1} \end{bmatrix} \quad (25)$$

equivalent to the system of equations given by Eq. (23), then the entire process of analytic continuation is reduced to a single matrix inversion

$$\begin{bmatrix} \mathbf{p} \\ \mathbf{q} \end{bmatrix} = X^{-1} \tilde{\sigma} \quad (26)$$

which provides the polynomial coefficients necessary to construct

$$\bar{\Sigma}_{(r)}(z) = \frac{\begin{bmatrix} 1 & z & z^2 & \cdots & z^{r-1} \end{bmatrix} \mathbf{p}}{\begin{bmatrix} 1 & z & z^2 & \cdots & z^{r-1} \end{bmatrix} \mathbf{q} + z^r}. \quad (27)$$

What we propose is that, having determined the p_n, q_n coefficients, we recover the λ_n, e_n coefficients and then use the criteria provided by Wall and Wetzel's theorem to determine whether the matrix inversion produced a $\bar{G}_{(r+1)}$ with an acceptable analytic form. As a first step, we investigate what can be learned from λ_1^2 , the first non-trivial J-fraction coefficient. λ_1^2 is equal to the sum of the residues of the poles in the self-energy and as such it gives the high frequency asymptotic behaviour of the self-energy via $\bar{\Sigma}_{(r)}(z) \sim \lambda_1^2/z$. A necessary condition for positive definiteness is that λ_1^2 be real and positive. We shall see that the convergence of $\text{Im} \lambda_1^2$ to zero as a function of the number r of poles in the Padé fitting function can provide information on the quality of the fit and on the analytic structure of the true continuation \bar{G} .

IV. NUMERICAL RESULTS

The procedure we have outlined in Sect. III is a specialization of the following general Padé procedure — such considerations are central to our statistical analysis of the quality of the fits provided by this method.

Given a function f and a set \mathcal{A} of $2r$ input points, we suppose that we can approximate the analytic continuation \bar{f} by a $[r-1/r]$ rational polynomial $\bar{f}_{(r)}$, the coefficients of which are determined by solving the linear

system of equations $\{\bar{f}_{(r)}(a) = f(a) : a \in \mathcal{A}\}$. This problem can be cast as a matrix inversion in which the kernel X has elements with ratios as large as

$$\zeta = |(\max \mathcal{A} \cup f(\mathcal{A}))^{r-1} / \min \mathcal{A} \cup f(\mathcal{A})|. \quad (28)$$

Thus to reliably perform the inversion we need a numerical range $\sim \zeta^2$, i.e. $2 \log_{10} \zeta$ decimal digits of numerical precision. This analysis is general in that no other Padé algorithm can have less stringent precision requirements.

For the case of a self-energy Σ , known at the first $2r$ Matsubara frequencies above the real line on the imaginary axis, we have shown that the matrix X is given by Eq. (25). Since $\Sigma(\omega_n) \sim 1/\omega_n$, the ratio of the largest to smallest terms in X is $\zeta = (\omega_{2r})^r = ((4r-1)\pi T)^r$, the square of which gives an estimate of the amount of precision needed to invert X . Here, that corresponds to

$$2r \log_{10}((4r-1)\pi T) \quad (29)$$

decimal digits.

To achieve a sufficient level of precision for our numerical work, we implement the Padé algorithm using the symbolic computation package MAPLE. Under MAPLE, expression evaluation takes place in software and thereby transcends the limits imposed by hardware floating-point. All computations are performed in base ten to any desired level of precision (we specified `Digits := 250`;¹⁰). Moreover, MAPLE is an ideal environment for rapid prototyping since high level matrix data types and routines are available as primitives.

We begin by considering a test function of known analytic structure. The self-energy¹¹

$$\Sigma(\vec{k}, \omega_n) = -\frac{U^2}{\beta M} \sum_{\vec{Q}} \sum_{\nu_{n'}} \chi^0(\vec{Q}, \nu_{n'}) G^0(\vec{Q} - \vec{k}, \nu_{n'} - \omega_n) \quad (30)$$

corresponds to the first ‘rung’ of the ladder diagrams in the T-matrix¹² approximation of the single-band Hubbard model¹³ (characterized by a near-neighbour hopping integral t and an on-site repulsion energy U). Here, G^0 is the free propagator

$$G^0(\vec{k}, \omega_n) = \frac{1}{i\omega_n - \xi_{\vec{k}}} \quad (31)$$

and χ^0 is the free pair susceptibility

$$\chi^0(\vec{Q}, \nu_n) = \frac{1}{\beta M} \sum_{\vec{k}} \sum_{\omega_{n'}} G^0(\vec{k}, \omega_{n'}) G^0(\vec{Q} - \vec{k}, \nu_n - \omega_{n'}). \quad (32)$$

The frequency sums in Eqs. (30) and (32) can be performed analytically, giving¹⁴

$$\chi^0(\vec{Q}, \nu_n) = \frac{1}{M} \sum_{\vec{k}} \frac{f[\xi_{\vec{k}}] + f[\xi_{\vec{Q}-\vec{k}}] - 1}{i\nu_n - \xi_{\vec{k}} - \xi_{\vec{Q}-\vec{k}}} \quad (33)$$

and

$$\Sigma(\vec{k}, \omega_n) = \frac{U^2}{M^2} * \quad (34)$$

$$\sum_{\vec{Q}, \vec{k}'} \frac{(f[\xi_{\vec{k}'}] + f[\xi_{\vec{Q}-\vec{k}'}] - 1)f[\xi_{\vec{Q}-\vec{k}}] - f[\xi_{\vec{k}'}]f[\xi_{\vec{Q}-\vec{k}'}]}{i\omega_n + \xi_{\vec{Q}-\vec{k}} - \xi_{\vec{k}'} - \xi_{\vec{Q}-\vec{k}'}}$$

Since the $\xi_{\vec{k}}$ are real, the analytic continuation of the self-energy is a meromorphic function with a finite number of simple poles, all situated along the real axis. Calculated in two dimensions on an 8×8 ($M = 64$) lattice, its $\vec{k} = 0$ component possesses $r_0 = 26$ poles. (The number of poles is determined by counting the number of distinct elements in the set $\{\xi_{\vec{Q}} - \xi_{\vec{k}'} - \xi_{\vec{Q}-\vec{k}'} : \forall \vec{k}', \vec{Q}\}$.)

For a particular set of parameters¹⁵ — we use an interaction strength $|U|/t = 4$, chemical potential $\mu/t = -1$, and temperature $T/t = 0.7$ — the test function, Eq. (30), is calculated in two different ways for the Matsubara frequencies $\{\omega_1, \omega_2, \dots, \omega_{2r}\}$. First, it is calculated exactly, as prescribed by Eq. (34), but with a small, random error, *viz.*, each value is multiplied by $1 + \epsilon$ with $-1 \leq \epsilon \leq 1$. Second, it is calculated by truncating the Matsubara sum at an arbitrary cutoff frequency $\nu_p \gg 1$ (much larger than the relevant energy scale of the problem) and then systematically adding back the high frequency contributions up to a given order. That is,

$$-\frac{1}{\beta} \sum_{\nu_{n'}} \chi^0(\vec{Q}, \nu_{n'}) G^0(\vec{Q} - \vec{k}, \nu_{n'} - \omega_n)$$

$$= -\frac{1}{\beta} \sum_{|\nu_{n'}| \leq \nu_p} \chi^0(\vec{Q}, \nu_{n'}) G^0(\vec{Q} - \vec{k}, \nu_{n'} - \omega_n) \quad (35)$$

$$+ \sum_{l=1}^{m-1} \chi_{(l)}^0(\vec{Q}) \Theta_{(l+1)}[i\omega_n + \xi_{\vec{Q}-\vec{k}}] + \mathcal{O}(1/(\nu_p)^m)$$

where

$$\chi_{(l)}^0(\vec{Q}) = \frac{1}{M} \sum_{\vec{k}} (f[\xi_{\vec{k}}] + f[\xi_{\vec{Q}-\vec{k}}] - 1)(\xi_{\vec{k}} + \xi_{\vec{Q}-\vec{k}})^{l-1} \quad (36)$$

are the coefficients of a Laurent expansion of $\chi^0(\vec{Q}, \nu_n)$ and the $\Theta_{(l)}$ functions (defined in the Appendix) are constructed using the symbolic manipulation capabilities of MAPLE.

Now, we let the self-energy, evaluated at the first $2r$ Matsubara frequencies according to the two schemes described above, serve as the input to the Padé procedure. The resulting approximant $\bar{\Sigma}_{(r)}$ yields a propagator $\bar{G}_{(r+1)}(\vec{k}, z) = (z - \xi_{\vec{k}} - \bar{\Sigma}_{(r)}(\vec{k}, z))^{-1}$ with spectral function $A_{(r+1)}(\vec{k}, \omega) = -(1/\pi) \text{Im} \bar{G}_{(r+1)}(\vec{k}, \omega + i0^+)$. The spectral function derived from the Padé approximant is compared to that of the exact function using the logarithmic measure

$$10^{-F} \equiv \int_{-\infty}^{\infty} dx (A(\vec{k}, x) - A_{(r+1)}(\vec{k}, x))^2 \quad (37)$$

$$= \frac{1}{\pi^2} \int_{-\infty}^{\infty} dx \left| \text{Im} \left(\bar{G}(\vec{k}, x + i\eta) - \bar{G}_{(r+1)}(\vec{k}, x + i\eta) \right) \right|^2.$$

In practice we choose η to be a small, but noninfinitesimal positive real quantity (we use $\eta/t = 0.064$), which has the effect of introducing a slight artificial broadening to the δ -function peaks of the spectral function.

The results of this comparison (for the $\vec{k} = 0$ component of the spectral function) are presented in Figs. 1(a) and 1(b), where F is plotted as a function of r for different values of the random error $E = -\log_{10} \epsilon$ and the systematic error $E = -\log_{10} 1/(\nu_p)^m = m \log_{10} \nu_p$ (and thus a larger E corresponds to a smaller error). In each graph, a vertical dashed line marks the exact number of poles ($r_0 = 26$) in the true self-energy. The most distinctive feature of both graphs is that, at high accuracy (large E), the F curves exhibit a large step at the point $r = r_0$. In the random error case, the $E = 120$ curve jumps by four decades, and this represents an improvement in the Padé fit of nearly 40 orders of magnitude. In the systematic error case, the result is even more dramatic: the $E = 100$ and $E = 120$ curves jump by roughly four and seven decades, respectively.

At these large accuracies, the only factor inhibiting the success of the Padé approximants is the lack of a sufficient number of poles to reproduce the analytic structure of the true function. The large jump observed in the large E curves marks the point, $r = r_0$, at which the number of poles in the Padé approximant exactly matches the required number, and for this and larger r there is no difficulty in finding an excellent fit of the test function. In contrast, when the input points are known to relatively low accuracy, no such feature is observed, and instead the F curves pass smoothly through r_0 . This makes clear that for self-energies calculated to 20, 40, or even 60 decimal digits of accuracy, the level of error in the input points is still the main obstacle to a successful Padé fit.

The usual response to this situation is to increase the number of Padé points in an attempt to overcome the intrinsic error limitations (by making the system of equations more and more overcomplete). However, whatever advantage this additional information brings to the Padé approximant is soon outweighed by the accompanying complications: When a rational polynomial of degree $[r - 1/r]$ is used to fit a function with $r_0 < r$ poles, $r - r_0$ zeros of the numerator must coincide with an equal number of zeros in the denominator in order to cancel the extraneous poles. As $r - r_0$ grows, it is less and less likely that this cancellation will be complete. A slight misplacement of zeros leads to ‘defects’ in which the function moves between 0 and ∞ in a small neighbourhood. Moreover, it cannot be predicted where these zero-zero pairs will appear¹⁷. For the purposes of calculating a spectral function, they are of little consequence provided that they lie deep in the complex plane. How-

ever, when they are not so far removed from the real axis, they can distort the spectral function away from its proper shape. When they lie on or near the real axis, they can give rise to deep troughs of negative spectral weight and other spurious, non-physical features.

The deterioration of the Padé fit, as described above, is evident in Figs. 1(a) and 1(b) in which many of the F curves reach maxima at points $r_{\text{best}} > r_0$ and then quickly begin to fall off for larger r . Interestingly, this behaviour is much more pronounced in the systematic error case where such maxima occur for each curve. In the random error case, the curves below some error threshold are essentially flat for all r .

The primary lesson that one should draw from these results is that the addition of Padé points well beyond the required number is not a useful strategy for improving the Padé fit. Unless the exact analytic continuation is already known, there is no way to predict the value of r_{best} . We believe that better results are achieved by fixing the number of Padé points at $2r_0$ (giving rise to a $[r_0 - 1/r_0]$ rational polynomial) and working towards increasing the accuracy with which those input points are calculated. Even a small effort there can result in an improvement of several orders of magnitude in the fit. What to try when one does not know *a priori* what r_0 is discussed later in this paper.

Now consider Figs. 2(a) through 2(d) in which the spectral function of a Padé approximant with 26 poles (calculated by specifying the value of the self-energy at 52 Matsubara frequencies) is compared to the exact spectral function. In Fig. 2(a), the accuracy of the input points is given by $E = 16$ (random error), roughly the number of digits in a double precision Fortran variable. Despite the fact that the overall energy scale is correct, the details of the fit are quite poor. Here, the effect of insufficient accuracy is to produce a washed out version of the spectral function which completely lacks fine structure. Even at $E = 30$ (Fig. 2(b)), corresponding to the number of digits available in the largest Fortran data type, the Padé inversion is only just beginning to distinguish the main peaks of the spectral function. Figure 2(c) shows the result for $E = 80$ and Fig. 2(d) the result for $E = 120$. Notice that in Fig. 2(d), the fit is near perfect: even the smallest peaks have been reproduced faithfully.

In this example, with $r = r_0$, the Padé approximant provides a remarkable fit to the true function whenever the accuracy of the input points is better than $E \sim 110$. The difficulty in translating our success in this specific case to the general problem is that, in real applications, one has no way to judge when sufficient accuracy has been achieved. Also, in most instances, the number of poles in the self-energy is unknown.

In what follows, we hope to address these deficiencies. We begin by defining a logarithmic measure of the imaginary part of the J-frac coefficient λ_1^2 :

$$10^{-\Lambda} \equiv |\text{Im } \lambda_1^2|. \quad (38)$$

We argued in Sect. III that λ_1^2 ought to be real and posi-

tive. In a Padé calculation, however, it is real-valued only to within some small fraction which characterizes the numerical sensitivity of the matrix inversion. As we shall soon discover, the convergence of the imaginary part of λ_1^2 to zero ($\Lambda \rightarrow \infty$) can be used (1) to determine when the threshold of accuracy for an exact fit has been reached and (2) to infer the value of r_0 if it is unknown.

In Figs. 3(a) and 3(b), we plot Λ as a function of r for the random and systematic error cases. Over each plot is superimposed a reference line given by Eq. (29). What we observe is a set of Λ curves that initially follow the reference line but later fan out, spaced according to their E values. Our claim is that these curves provide the quantitative measure of success of the Padé approximant that has heretofore been lacking, the essential point being that the shape of the curves reveals the performance characteristics of the Padé inversion in the various r regimes.

When $0 < r < r_0$, the accuracy of the Padé approximant is matrix inversion dominated and the behaviour of Λ is governed by $\Lambda \sim 2r \log_{10}(4r - 1)\pi T$. In this regime, the Padé approximant has too few poles to fit the true function and thus the matrix inversion must judiciously arrange the available poles (sometimes apportioning one pole to a region where there should be two or three) to give the best possible fit. In the opposite limit, $r \gg r_0$, the accuracy of the Padé approximant is input-point error dominated. In this regime, there are more than enough poles to perform an exact fit, but the proper placement of those poles and the determination of their residues is hampered by the finite accuracy to which the input points are known. We find this reflected in the Λ curves which, for large r , saturate at a value $\Lambda \sim E$ (roughly).

Most interesting, though, is the behaviour of Λ in the vicinity of $r = r_0$ where the Λ curves in Figs. 3(a) and 3(b) first cross the reference line. In those plots, we see that the Λ curves corresponding to small values of E closely follow the reference line (Eq. (29)) until finite accuracy becomes a limiting factor. The curves then fall below the reference line and become more or less flat. As E is increased, the r coordinate at which a given Λ curve first deviates from the reference line moves to the right until (for some accuracy, E_0 say) it coincides with r_0 . Here, there is a sudden change in behaviour: all Λ curves corresponding to accuracies $E > E_0$ cross the reference line at $r = r_0$. Such a crossing signals that there are now both sufficient poles in the approximant and sufficient accuracy on the input points to fit $\bar{\Sigma}$ more or less exactly. We can verify this interpretation by appealing to Figs. 1 and 2 which clearly show a large jump at r_0 for precisely the same curves that demonstrate a crossing in Figs. 3(a) and 3(b).

The results we have described are extremely general and do not depend on the choice of test function. For example, we may replace Eq. (30) with the full non-self-consistent T-matrix self-energy

$$\Sigma(\vec{k}, \omega_n) = -\frac{U^2}{\beta M} \sum_{\vec{Q}} \sum_{\nu_{n'}} \frac{\chi^0(\vec{Q}, \nu_{n'}) G^0(\vec{Q} - \vec{k}, \nu_{n'} - \omega_n)}{1 + U \chi^0(\vec{Q}, \nu_{n'})}. \quad (39)$$

Here, the frequency sums cannot be performed analytically¹⁶ and thus we do not have a closed form analytical expression for the self-energy. (Thus, this is more representative of the usual situation in which the Padé method might be applied.) In this case, we know only that its analytic continuation has a finite number of poles along the real axis (although we are able to predict analytically an upper bound for the number of poles).

This self-energy can be calculated to high accuracy using the method of Eq. (35) with the $\chi_{(l)}^0(\vec{Q})$ replaced by the coefficients of the Laurent expansion of $\chi^0(\vec{Q}, \nu_n)/(1 + U \chi^0(\vec{Q}, \nu_n))$. That is, $\chi_{(1)}^0(\vec{Q}) \mapsto \chi_{(1)}^0(\vec{Q})$, $\chi_{(2)}^0(\vec{Q}) \mapsto \chi_{(2)}^0(\vec{Q}) - U \chi_{(1)}^0(\vec{Q})^2$ and so on according to

$$\begin{aligned} & \frac{\frac{\chi_{(1)}}{i\nu_n} + \frac{\chi_{(2)}}{(i\nu_n)^2} + \frac{\chi_{(3)}}{(i\nu_n)^3} + \dots}{1 + U \left(\frac{\chi_{(1)}}{i\nu_n} + \frac{\chi_{(2)}}{(i\nu_n)^2} + \frac{\chi_{(3)}}{(i\nu_n)^3} + \dots \right)} \\ &= \frac{\chi_{(1)}}{i\nu_n} + \frac{\chi_{(2)} - U \chi_{(1)}^2}{(i\nu_n)^2} + \frac{\chi_{(3)} - 2U \chi_{(2)} \chi_{(1)} + U^2 \chi_{(1)}^3}{(i\nu_n)^3} + \dots \end{aligned} \quad (40)$$

This expansion is easy to implement in MAPLE using the `series()` command, although the computational resources required to execute it are significant due to the combinatorial explosion of terms at high order.

The Padé approximant method can then be applied to Eq. (39) calculated in this way. We find that the resulting plot of Λ vs. r is identical to that of Fig. 3(b) except that the crossing of the reference line at high accuracy now occurs at $r = 156$. This allows us to deduce that the function has $r_0 = 156$ poles, significantly more than the 26 poles of Eq. (34). (This is a consequence of the lifting of degeneracy in each \vec{Q} component brought about by the renormalization $1/(1 + U \chi^0(\vec{Q}, \nu_n))$.) We also find that the approximant spectral function compares well with increasing accuracy of the input points to the numerically exact spectral functions as calculated (i) by a non-Padé method due to Marsiglio et al.¹⁸ (this non-Padé method is of limited application since it requires the self-energy to have a very specific form, but for those cases where it is applicable, it can outperform the Padé method), and (ii) by a partial fraction decomposition of the self energy¹⁹ that can be done to a very high accuracy (say 10^{-40} on all poles and residues).

Finally, one interesting feature that could potentially be exploited is that for self-energy values calculated using the Θ function expansion, the value of r which gives the maximum value of Λ roughly tracks r_{best} (cf. Figs. 1(b) and 3(b)).

V. CONCLUSIONS

The Padé procedure is very sensitive to the numerical precision with which the matrix inversion is performed and to the intrinsic error on the input points. Sufficient precision is difficult to achieve in traditional computer languages (e.g. C, Fortran) and so, in many instances, it may be necessary to make use of a symbolic computation package capable of supporting very large precision data types. Likewise, sufficient accuracy is difficult to achieve without a sophisticated computational scheme (e.g. the Θ function expansion) that goes beyond a simple truncation of the Matsubara frequency sums in the self-energy. The required level of precision and accuracy depends on the temperature T , which controls the spacing of the Matsubara points, and on the pole count r_0 .

An insufficient level of accuracy leads to an approximant spectral function that lacks fine structural detail or, worse, one that exhibits spurious spikes or troughs of spectral weight. This poses a problem whenever we are interested in the presence of a specific feature in the spectral function (e.g. the onset of a normal state pseudogap). In that case, it is essential to have confidence in the quality of the Padé result. We must be convinced that the observed feature is robust and not merely a by-product of insufficient accuracy.

We have argued that simply adding more Padé points cannot compensate for too large an error on the input points. While there is a small set of r values for which an increase in r improves the fit, there is no known criterion that indicates when to stop adding points. Without already knowing the exact result, one cannot distinguish between the regime where additional points improve the fit ($r < r_{\text{best}}$) and the regime where such points degrade it ($r \geq r_{\text{best}}$). Instead, we recommend the use of a Padé approximant function having the same number of poles as the function to be fit. The exact number of poles, when it is not known, can be determined from the crossing point in a Λ vs. r plot. The crossing also indicates that a sufficient level of numerical accuracy in the input points has been achieved.

There are several caveats to the procedure we have outlined. (1) If the true Green's function has a branch cut along the real axis arising from transcendental functions then no Λ crossing will ever be observed, since a branch cut of that kind can only be represented by an infinity of poles ($r_0 = \infty$). (2) The self-energy of the Green's function we are trying to reproduce must have the correct asymptotic form and must be analytic in, say, the upper half of the complex plane; otherwise, the rational polynomial (or continued fraction) form of the approximant cannot reproduce its analytic structure. (3) The Padé method is often used to model a function that is smooth in some region of interest (well away from its poles) and such calculations are rarely performed with more than machine accuracy. Our numerical analysis of the Padé inversion, with its prediction of extremely high accuracy

requirements, is not meant to invalidate these results. We have applied the Padé method to the particularly difficult problem of reproducing the sharp peak structures characteristic of a spectral function whose Green's function has its poles along the real axis. In that case, the poles lie in the region of interest. The precision and accuracy requirements of the Padé inversion are greatly reduced if the poles of the Green's function lie deep in the complex plane.

Finally, let us remember that the starting point for our new Padé approach was the realization that the convergence of the continued fraction coefficients to 'allowed' values can provide a criterion for judging the quality of a Padé approximant, even if the analytic structure of the function we are trying to fit is unknown. In Sect. IV, we demonstrated the utility of this idea using the λ_1 coefficient. However, we know that there is much additional information that can be extracted from the remaining continued fraction coefficients. In future, perhaps our analysis can be extended to include e_1 , λ_2 , e_2 , etc.

ACKNOWLEDGMENTS

One of us (RJG) wishes to thank George Baker for directing him to a variety of valuable references, and we thank David Sénéchal and André-Marie Tremblay for helpful comments on their recent paper⁶. This work was supported by the NSERC of Canada, and the Institute of Theoretical Physics of the University of Alberta.

APPENDIX:

In addition to the usual occupation functions

$$f[x] = \frac{1}{\beta} \sum_{\omega_n} \frac{e^{i\omega_n 0^+}}{i\omega_n - x} = \frac{1}{e^{\beta x} + 1} \quad (\text{A1a})$$

$$b[x] = -\frac{1}{\beta} \sum_{\nu_n} \frac{e^{i\nu_n 0^+}}{i\nu_n - x} = \frac{1}{e^{\beta x} - 1} \quad (\text{A1b})$$

it is often convenient to define *partial* occupation functions. For example, the bose version of such a function looks like

$$\tilde{b}[x] = -\frac{1}{\beta} \sum_{\nu_n > \nu_p} \frac{e^{i\nu_n 0^+}}{i\nu_n - x} = \frac{1}{2\pi i} \psi \left(\frac{\beta}{2\pi i} (i\nu_{p+1} - x) \right) \quad (\text{A2})$$

where $\psi(z) = d \ln \Gamma(z) / dz$ is the digamma function²⁰. This can be generalized to a m -order function (symmetric in its arguments)

$$\tilde{b}[x_1, x_2, \dots, x_m] = -\frac{1}{\beta} \sum_{\nu_n > \nu_p} \frac{1}{i\nu_n - x_1} \frac{1}{i\nu_n - x_2} \dots \frac{1}{i\nu_n - x_m} \quad (\text{A3})$$

which has the interesting property that it can be expressed (via partial fraction decomposition) in terms of the $(m-1)$ -order partial occupation function

$$\begin{aligned} & \tilde{b}[x_1, x_2, \dots, x_m] \quad (\text{A4}) \\ &= \begin{cases} \frac{\tilde{b}[x_1, x_2, \dots, x_{m-2}, x_{m-1}] - \tilde{b}[x_1, x_2, \dots, x_{m-2}, x_m]}{x_{m-1} - x_m} & \text{if } x_{m-1} \neq x_m \\ \frac{\partial}{\partial y} \tilde{b}[x_1, x_2, \dots, x_{m-2}, y] \Big|_{y=x_m} & \text{otherwise.} \end{cases} \end{aligned}$$

Equation (A2) serves to terminate the recursion.

Furthermore, it is straightforward to show that for all $l \geq 0$

$$\begin{aligned} \Theta_{(l+2)}[x] &\equiv -\frac{1}{\beta} \sum_{|\nu_n| > \nu_p} \frac{1}{(i\nu_n)^{l+1}} \frac{1}{i\nu_n - x} \\ &= -\frac{1}{\beta} \sum_{\nu_n > \nu_p} \left(\frac{1}{(i\nu_n)^{l+1}} \frac{1}{i\nu_n - x} + \frac{1}{(-i\nu_n)^{l+1}} \frac{1}{-i\nu_n - x} \right) \\ &= \tilde{b}[\underbrace{0, 0, \dots, 0}_{l+1}, x] + (-1)^l \tilde{b}[\underbrace{0, 0, \dots, 0}_{l+1}, -x] \\ &= \frac{1}{l!} \frac{\partial^l}{\partial y^l} \left\{ \tilde{b}[x, y] + (-1)^l \tilde{b}[-x, y] \right\} \Big|_{y=0} \quad (\text{A5}) \end{aligned}$$

where, according to Eq. (A4), the two-argument function $\tilde{b}[x, y]$ is related to $\tilde{b}[x]$ by

$$\tilde{b}[x, y] = \frac{\tilde{b}[x] - \tilde{b}[y]}{x - y} \quad (\text{A6})$$

provided $x \neq y$. The Θ functions provide a closed-form representation of the high-frequency asymptotics of a broad class of Matsubara sums. In particular, the sum

$$-\frac{1}{\beta} \sum_{\nu_{n'}} \chi^0(\vec{Q}, \nu_{n'}) G^0(\vec{Q} - \vec{k}, \nu_{n'} - \omega_n) \quad (\text{A7})$$

can be separated into a finite sum over all 'low' frequencies

$$\frac{1}{\beta} \sum_{|\nu_{n'}| \leq \nu_p} \chi^0(\vec{Q}, \nu_{n'}) G^0(\vec{Q} - \vec{k}, \nu_{n'} - \omega_n) \quad (\text{A8})$$

and an infinite sum over the remaining frequencies

$$\begin{aligned} & -\frac{1}{\beta} \sum_{|\nu_{n'}| > \nu_p} \chi^0(\vec{Q}, \nu_{n'}) G^0(\vec{Q} - \vec{k}, \nu_{n'} - \omega_n) \\ &= -\frac{1}{\beta} \sum_{|\nu_{n'}| > \nu_p} \left(\sum_{l=1}^{\infty} \frac{\chi_{(l)}^0(\vec{Q})}{(i\nu_{n'})^l} \right) \frac{1}{i(\nu_{n'} - \omega_n) - \xi_{\vec{Q}-\vec{k}}} \quad (\text{A9}) \\ &= -\sum_{l=1}^{\infty} \chi_{(l)}^0(\vec{Q}) \frac{1}{\beta} \sum_{|\nu_{n'}| > \nu_p} \frac{1}{(i\nu_{n'})^l} \frac{1}{i\nu_{n'} - (i\omega_n + \xi_{\vec{Q}-\vec{k}})} \\ &= +\sum_{l=1}^{\infty} \chi_{(l)}^0(\vec{Q}) \Theta_{(l+1)}[i\omega_n + \xi_{\vec{Q}-\vec{k}}] \end{aligned}$$

where, in Eq. (A9), we have used the fact that the free susceptibility χ^0 admits a Laurent expansion in the frequency variable

$$\begin{aligned}\chi^0(\vec{Q}, \nu_n) &= \frac{1}{i\nu_n} \frac{1}{M} \sum_{\vec{k}} \frac{f[\xi_{\vec{k}}] + f[\xi_{\vec{Q}-\vec{k}}] - 1}{1 - (\xi_{\vec{k}} + \xi_{\vec{Q}-\vec{k}})/i\nu_n} \\ &= \frac{\chi_{(1)}^0(\vec{Q})}{i\nu_n} + \frac{\chi_{(2)}^0(\vec{Q})}{(i\nu_n)^2} + \frac{\chi_{(3)}^0(\vec{Q})}{(i\nu_n)^3} + \dots\end{aligned}\quad (\text{A10})$$

with \vec{Q} -dependent coefficients

$$\chi_{(l)}^0(\vec{Q}) = \frac{1}{M} \sum_{\vec{k}} (f[\xi_{\vec{k}}] + f[\xi_{\vec{Q}-\vec{k}}] - 1)(\xi_{\vec{k}} + \xi_{\vec{Q}-\vec{k}})^{l-1}.\quad (\text{A11})$$

[†] Address as of Sept. 1, 1999: Dept. of Physics, Massachusetts Institute of Technology, Cambridge MA 02139.

¹ Of course, other methods are available, for certain formulations of the many-body, thermal Green's function problem. A number of these are discussed in a recent paper: see J. Schmalian, M. Langer, S. Grabowski and K.H. Bennemann, *Comp. Phys. Comm.* **93**, 141 (1996), and references therein.

² G. A. Baker, *Essentials of Padé Approximants*, Academic Press, New York (1975).

³ H. J. Vidberg and J. Serene, *J. Low Temp. Phys.* **29**, 179 (1977).

⁴ G. Baym and D. Mermin, *J. Math. Phys.* **2**, 232 (1961).

⁵ H. S. Wall, *Analytic theory of continued fractions*, Chelsea Publishing Co., New York (1948).

⁶ The implementation of such a form was made recently in S. Pairault, D. Sénéchal, and A.-M. S. Tremblay, *Phys. Rev. Lett.* **80**, 5389 (1998); also see cond-mat/9905242.

⁷ Note that we have chosen to absorb all frequency independent terms of the self-energy into ξ .

⁸ H. S. Wall and M. Wetzel, *Trans. Amer. Math. Soc.* **55**, 373 (1944).

⁹ The system of equations is linear in the (p, q) basis, but not in the (λ, e) basis.

¹⁰ There is no reason to choose this specific value. Any **Digits** which is in excess of what is required by the statistical test discussed in this section is adequate. It is important to note that there is virtually no extra time required to make such high accuracy calculations, and thus there is no reason to not implement algorithms such as this with a very high accuracy.

¹¹ We use the convention that $\omega_n = (2n - 1)\pi/\beta$ represents a fermionic Matsubara frequency and $\nu_n = 2n\pi/\beta$ a bosonic one.

¹² See, *e.g.*, A.L. Fetter and J.D. Walecka, "Quantum Theory of Many-Particle Systems" (McGraw Hill, New York, 1971).

¹³ For those cave dwellers not familiar with the Hubbard model, an excellent discussion may be found in A. Auerbach, "Interacting Electrons and Quantum Magnetism" (Springer-Verlag, New York, 1994).

¹⁴ These relations can be derived most easily using the identity $(1 - f(x) - f(y)) * N(x + y) = f(x) * f(y)$, where f/N is the fermi/bose distribution function.

¹⁵ As viewed in the μ - T phase diagram, this choice of parameters places the system well inside the band ($-4 < \mu/t < 4$) and just above the superconducting instability ($T > T_c$), the so-called Thouless criterion line. This region is of interest in that one expects to see a suppression of the spectral weight around the chemical potential, the so-called normal state pseudo-gap.

¹⁶ In fact, the frequency sum can be performed formally to yield an infinite sum of generalized occupation functions. However, this is of no computational value since it only trades a difficult frequency sum for an infinite series of increasingly more difficult (at each order) \vec{k} sums.

¹⁷ Theorems do exist concerning their overall distribution in the complex plane; see Chapt. 11 and 13 of Ref.².

¹⁸ F. Marsiglio, M. Schossmann, and J. P. Carbotte, *Phys. Rev. B* **39**, 4965 (1988).

¹⁹ The details of these calculations will be presented in a separate publication.

²⁰ L. V. Ahlfors, *Complex Analysis*, McGraw-Hill Book Co., New York (1953).

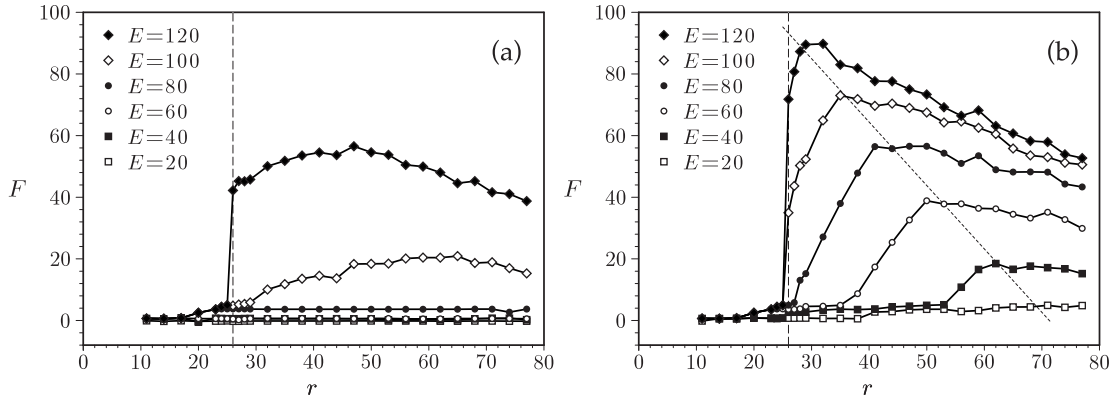


FIG. 1. For various levels of (a) random and (b) systematic error, characterized roughly as 10^{-E} (see the text for more details), the quality of the Padé fit as measured by F (see Eq. (37)) is plotted with respect to the number of poles in the Padé approximant (the solid lines are a guide to the eye). The self energy being studied is that of Eq. (30) where the parameters of the attractive Hubbard model (with t being the hopping energy), for an 8×8 square lattice, are a repulsive energy $|U|/t = 4$, a chemical potential $\mu/t = -1$, and a temperature $T/t = 0.7$. The vertical dashed line indicates the number of poles ($r_0 = 26$) in the true Green's function. In plot (a), error bars (representing the standard deviation of the data points over a set of initial random seeds) are smaller than the symbols marking the data points and are not shown. In plot (b), the dotted line is the best linear fit through the maximum values of F .

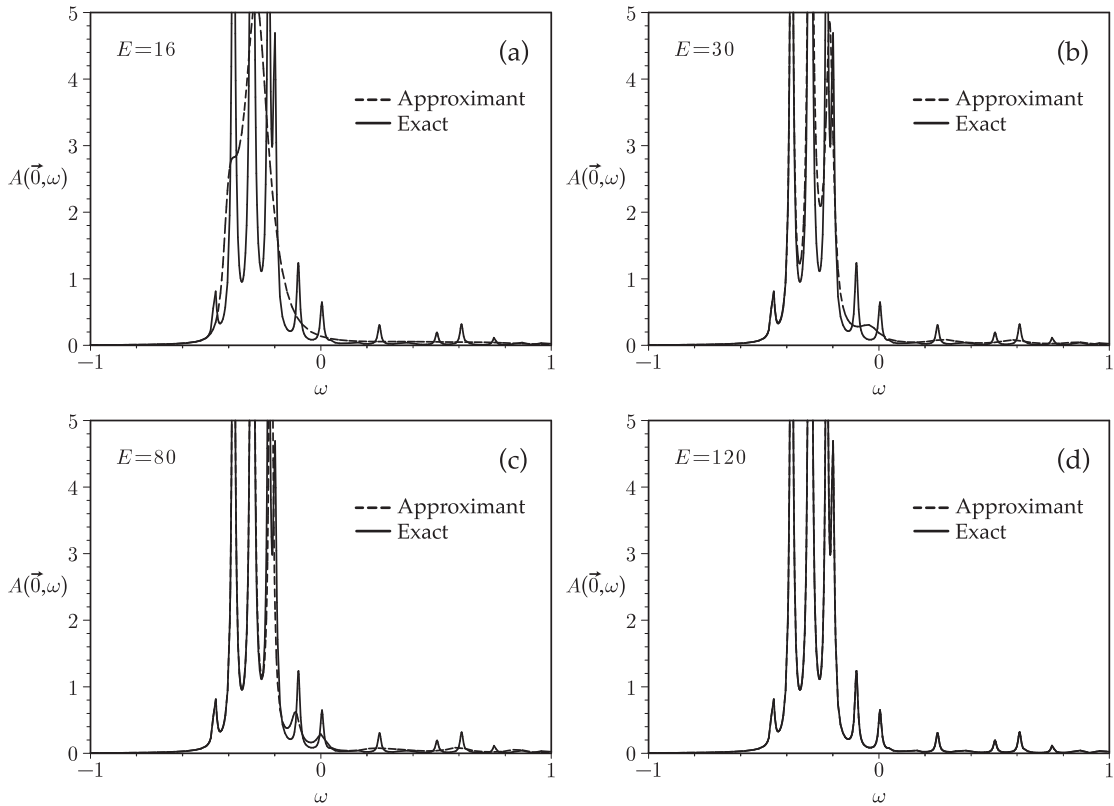


FIG. 2. The spectral function of the Padé approximant is compared to the exact spectral function for different levels of random error (10^{-E}) on the initial input points. The parameters of the Hamiltonian and the self-energy being studied are the same as those of Fig. 1.

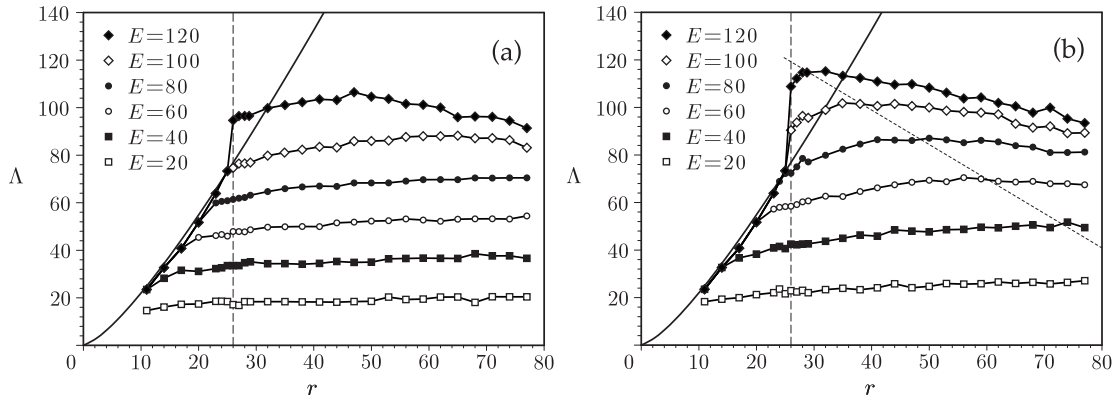


FIG. 3. For various levels of (a) random and (b) systematic error (10^{-E}), the parameter Λ is plotted with respect to the number of poles in the Padé approximant. The parameters are the same as those of Fig. 1. The vertical dashed line indicates the number of poles ($r_0 = 26$) in the true Green's function. The solid line originating in the lower left corner is given by $2r \log 10(4r - 1)\pi T$. In plot (b), the dotted line is the best linear fit through the maximum values of Λ . The parameters of the Hamiltonian and the self-energy being studied are the same as those of Fig. 1.